HHS Public Access

Author manuscript

Cell. Author manuscript; available in PMC 2015 November 20.

Published in final edited form as:

Cell. 2014 November 20; 159(5): 1027–1041. doi:10.1016/j.cell.2014.10.023.

ER contact sites define the position and timing of endosome fission

Ashley A. Rowland[*], **Patrick J. Chitwood**[*], **Melissa J. Phillips**, and **Gia K. Voeltz**[†]

Department of Molecular, Cellular, and Developmental Biology, University of Colorado,Boulder, CO 80309, USA

Summary

Endocytic cargo and Rab GTPases are segregated to distinct domains of an endosome. These domains maintain their identity until they undergo fission to traffic cargo. It is not fully understood how segregation of cargo or Rab proteins is maintained along the continuous endosomal membrane, or what machinery is required for fission. Endosomes form contact sites with the ER that are maintained during trafficking. Here, we show that stable contacts form between the ER and endosome at constricted sorting domains and that free diffusion of cargo is limited at these positions. We demonstrate that the site of constriction and fission for early and late endosomes is spatially and temporally linked to contact sites with the ER. Lastly, we show that altering ER structure and dynamics reduces the efficiency of endosome fission. Together these data reveal a surprising role for ER contact in defining the timing and position of endosome fission.

Introduction

The endocytic pathway is used to internalize components present on the plasma membrane and in the extracellular fluid. After internalization, endocytosed cargo is sorted at multiple steps during trafficking. Cargo destined for degradation at the lysosome is sorted away from both recycled cargo destined for the plasma membrane and cargo trafficked to the Golgi. The sorting of these cargoes must occur prior to endosome fission, and multiple machineries and mechanisms have been identified that contribute to this process (Hanyaloglu and von Zastrow, 2008; Maxfield and McGraw, 2004; Seaman, 2008). Microtubules and their motor proteins, branched actin networks generated by the Arp2/3 activator WASH, the retromer, and structural membrane shaping proteins such as sorting nexins (SNX), have all been implicated in endosome structure and cargo sorting (Gautreau et al., 2014; Hunt et al., 2013;

[†]Correspondence to: gia.voeltz@colorado.edu.
[*]These authors contributed equally to this work.

Author Contributions:
A.A.R, P.J.C., and G.K.V. contributed to experimental design. A.A.R and P.J.C conducted all experiments, data analysis, and figure composition. M.J.P generated expression constructs and assisted with experiments. A.A.R. and G.K.V wrote the manuscript. A.A.R, P.J.C., M.J.P., and G.K.V. proofed the manuscript.

Puthenveedu et al., 2010). However, it is not known what regulates the timing and position of membrane fission to separate the sorted compartments.

Functional contact sites have been observed between the ER and endosomes (Alpy et al., 2013; Eden et al., 2010; Rocha et al., 2009). Measurements by electron microscopy and tomography have revealed that contact sites between the ER network and individual endosomes exist at multiple discrete positions around the endosome, which additively covers only ~5% of the endosome surface area (Alpy et al., 2013; Friedman et al., 2013). Despite the abundance and discrete nature of these contacts, they appear to be tightly coupled since the two organelles maintain contact even as they are trafficked on the microtubule network (Friedman et al., 2013; Zajac et al., 2013). Endosomes become bound to the ER early in their biogenesis and this association increases with maturation: we found >99% of late endosomes are tightly associated with the ER as they traffic, in contrast to ~50% of early endosomes (Friedman et al., 2013). Thus, ER contact could regulate the biogenesis of endosomes or become targeted to endosomes following a maturation step. Once established, ER contact with endosomes is often maintained despite trafficking, and this suggests important functions occur at the interface.

Two functions have been demonstrated to occur at the ER-endosome interface (van der Kant and Neefjes, 2014). Interactions between (VAMP)-associated protein A (VAP-A) on the ER and the endosome localized partners are thought to regulate cholesterol sensing and lipid transfer. For example, the endosomal protein ORP1L interacts with VAP-A under low cholesterol conditions which could allow for cholesterol exchange, thereby acting as a sensor (Rocha et al., 2009). ER-endosome contact also occurs via the ER-localized phosphatase, PTP1B, which interacts with EGFR, dephosphorylating it to promote incorporation into intraluminal vesicles, a necessary step for EGFR degradation by the lysosome (Eden et al., 2010). Several recent papers also suggest that late endosomes may take up Ca^{2+} from ER stores during their maturation process, however, it remains to be determined whether Ca^{2+} is directly transferred at the interface (Kilpatrick et al., 2013; López-Sanjurjo et al., 2013; Morgan et al., 2013).

The ER also forms contacts with several other organelles (Helle et al., 2013), and its role at these various sites may be analogous. At mitochondria and the plasma membrane, the ER provides Ca^{2+} in different functional contexts (Elbaz and Schuldiner, 2011). Emerging evidence also shows lipids are modified or transferred at the ER interface (Stefan et al., 2013; Toulmay and Prinz, 2011). Recently, we discovered that endoplasmic reticulum (ER) tubules circumscribe mitochondrial constrictions and define the position of mitochondrial fission (Friedman et al., 2011). We predicted that mechanisms of membrane fission may also be conserved between various organelles. Here we hypothesized and tested whether ER contacts define the timing and the position of endosome fission. To test this, we visualized Rab partitioning, cargo sorting, and endosome fission relative to the ER network in live Cos-7 cells.

Results

Dynamic ER Tubules Make Contact with Early Endosome Fission Sites

To visualize early endosome sorting and fission events relative to the ER, cells were co-transfected with GFP-Rab4, mCh-Rab5, and with the general ER marker BFP-Sec61β and were imaged by live confocal fluorescence microscopy (Figure 1A and D). Rab4 localizes to both the vacuolar and budding compartment of the early endosome (Sönnichsen et al., 2000), while Rab5 is exclusively localized to the vacuolar compartment (Sönnichsen et al., 2000; Trischler et al., 1999). Partitioning of cargo also occurs within the early endosome sorting domains. To ensure that the endosomes we visualized were functional, cells were pulse-labeled with Epidermal Growth Factor (EGF) (Figure 1A-C) or Transferrin (Tf) (Figure 1D-F) cargo conjugated to Alexa Fluor® 647. The Rab4 and Rab5 endosomes contain labeled cargo and their localization and morphology is consistent with previous reports (Sönnichsen et al., 2000; Trischler et al., 1999) (Figure 1A and D).

Upon fission, a smaller $Rab4^+$ compartment buds off of a larger $Rab4^+/Rab5^+$ vacuolar compartment (Figure 1B and E, top panels, Movie S1 and S2). The fluorescent EGF is confined to the vacuolar $Rab4^+/Rab5^+$ compartment and does not enter into the bud (see Figure 1B, panel row 3, yellow arrowhead, and Movie S1). In contrast, Tf was not confined to a compartment and was found in the $Rab4^+$ bud as well as the $Rab4^+/Rab5^+$ compartment (Figure 1E, panel row 3,yellow arrowhead, Movie S2). Live cell imaging (Figure 1B and E) and the corresponding line-scan analysis (Figure 1C and F) reveals that in both examples, an ER tubule moves into position at the divide between the two pre-formed compartments just before fission occurs (compare the position of the ER tubule relative to the two sorting compartments in the Pre-ER and Pre-Fission images and line-scans). These data reveal that ER tubules mark the position of early endosome fission and that there is a temporal relationship between ER recruitment and fission.

ER Tubules Contact Sorting Domains on Early Endosomes

It is difficult to quantitate whether the ER marks all early endosome fission events because early endosomes are small and fission is rapid, hindering our ability to capture instances of clear constriction followed by fission. Thus, we sought ways to slow fission and/or inhibit it at intermediate stages to better resolve the relationship between ER tubules and the position of early endosome constriction and fission. This was accomplished by treating cells with dynasore, a drug which has been shown to inhibit Dynamin-1, Dynamin-2, and Drp1 *in vitro* (Kirchhausen et al., 2008; Macia et al., 2006). As previously reported (Derivery et al., 2009; Mesaki et al., 2011), Cos-7 cells treated with dynasore accumulate tubular early endosomes (Figure 2A). This phenotype could be a consequence of dynamin inhibition or it could be due to off-target effects, which have been reported (Park et al., 2013). However, our data demonstrate that dynasore treatment is a very useful tool to slow the process of endosome fission and image bona fide fission intermediates at ER contact sites.

Cells were co-transfected with markers of early endosomes (mCh-Rab5) and the ER (GFP-Sec61β) and were treated with dynasore just prior to imaging. Treatment led to the formation of elongated $Rab5^+$ endosomes and did not alter the structure of the ER (Figure

2A) (Derivery et al., 2009; Mesaki et al., 2011). Like untreated endosomes, dynasore-induced tubular endosomes contain both degraded and recycled cargo that partition as expected (Figure S1A and S1B). To further test if tubular endosomes had features characteristic of native endosomes, we investigated whether they contained domains marked by the WASH complex (Figure 2). WASH is a multi-protein complex that activates Arp2/3-mediated actin nucleation at sorting domains (Derivery et al., 2009; Gomez and Billadeau, 2009; Harbour et al., 2012; Jia et al., 2010), and this actin nucleation may participate in cargo sorting (Puthenveedu et al., 2010), or generate force to catalyze fission. To mark the complex, we tagged FAM21, which has been shown to localize to early endosomes, bind the retromer complex, and regulate recruitment of WASH to endosomal sorting domains (Seaman et al., 2013). Cells were co-transfected with GFP-Rab5, BFP-Sec61β, and mCh-FAM21. In dynasore treated cells, FAM21 localized to patches and punctate structures along tubular endosomes (Figure 2B). Line-scan analysis demonstrated that FAM21-labeled structures corresponded to positions where Rab5 fluorescence was minimal, indicative of a constriction (see arrows in Figure 2C and D). ER tubules also crossed over the positions of FAM21-marked constrictions (see arrows in Figure 2C and D). These data demonstrate that sorting domains localize to dynasore-induced elongated endosomes and ER tubule crossings are spatially linked to these domains.

ER Tubules Contact Endosomes at a Barrier to Cargo Diffusion

Our data suggest that dynasore treatment can stall fission at ER-marked endosome sorting domains, and line-scan analysis indicates endosomes are constricted at ER contact sites (Figure 2D). To further establish the importance of the ER at stalled constrictions, we reasoned a functional constriction has the potential to impede the diffusion of cargo. According to the bulkflow hypothesis, membrane-bound cargo that is recycled to the plasma membrane, like Transferrin Receptor (TfR), diffuses freely in the membrane (Dunn et al., 1989; Mayor et al., 1993). We designed photobleaching techniques to test whether a diffusion barrier exists at minimums in fluorescence intensity, which would reflect a functional constriction at ER contact sites (see model Figure 2E). Cells were co-transfected with an ER marker (mCh-Sec61β), an early endosomal marker (BFP-Rab5) and a membrane-bound cargo marker (GFP-TfR). Next, cells were treated with dynasore to generate elongated endosomes. We photobleached GFP-TfR at one end of a tubular endosome and then visualized fluorescence recovery from the unbleached direction (see model Figure 2E). To confirm tubular endosomes persist throughout this process, we co-visualized unbleached BFP-Rab5. Two examples of TfR fluorescence recovery along the tubular endosome are shown in kymographs (Figure 2F and H). In example 2F, the GFP-TfR is photobleached as indicated (in the yellow circle), and the fluorescent signal recovers rapidly (within 10s) up to a position marked by the yellow arrow. This position corresponds to a contact site with the tip of an ER tubule (see merge with the ER on the right). Furthermore, line-scan analysis demonstrates that the endosome constriction (Rab5) and the diffusion barrier overlap with the ER contact site even as the endosome moves over time (Figure 2G, yellow arrows mark the diffusion barrier [D.B.], also see Movie S3). In example 2H, recovery is also rapid up to the position marked by a yellow arrow, which corresponds to a crossing ER tubule. As before, diffusion was limited at the position corresponding to a minimum in Rab5 fluorescence on the endosome, confirming that it is indeed a constriction

(Figure 2H-I). This suggests that the bulk flow of cargo between compartments is restricted at ER-marked constrictions prior to endosome fission.

Fission of Tubular Early Endosomes Occurs at ER Contact Sites

ER association with tubular endosome constrictions is strikingly reminiscent of contact sites between ER tubules and mitochondrial constrictions that undergo fission (Friedman et al., 2011). We therefore tested if ER-marked constrictions along tubular endosomes are stalled intermediates primed to undergo fission. Cells were co-transfected with mCh-Rab5 and GFP-Sec61β then treated with dynasore to generate tubular endosomes. To capture fission, dynasore was inactivated with fetal bovine serum (FBS) and cells were imaged live (Figure 3A). As with native early endosomes, the ER contacted elongated endosomes and defined the position of constriction and fission (Figure 3B and C). We visualized 31 individual fission events (in 9 cells, Fig.3D, Movie S4). ER tubule crossings were present at 80.6% of these fission events (Figure 3D). The mean coverage of the ER network on the tubular endosomes analyzed was 22.36% (Figure 3E and F), which demonstrates that ER contact at the site of fission is not due to chance. Together these data show that ER contact sites are spatially linked to the position of constriction and fission on early sorting endosomes.

ER Recruitment is Spatially and Temporally Linked to the Position of Late Endosome Fission

The vast majority of late endosomes (>99%) are also tightly associated with the ER over time (Friedman et al., 2013). We asked whether ER contact sites are also spatially linked to the position of late endosome fission. Cos-7 cells were transfected with markers for late endosomes (mCh-Rab7) and the ER (GFP-Sec61β) and were imaged live by confocal fluorescence microscopy. Exogenous mCh-Rab7 was expressed at levels similar to endogenous (Figure S2A), and the morphology of labeled late endosomes matched previous reports (Figure 4A and Figure S2B) (Barbero et al., 2002). Cells were also pulse-labeled with EGF (conjugated to Alexa Fluor® 647) to mark the internalization and segregation of cargo. We imaged the structure, dynamics, and interactions between the endosomes and the ER over time at the periphery of the cell where both organelles are well resolved. A representative example of a late endosome that undergoes fission is shown in Figure 4B and Figure S2C. Here, a small $Rab7^+$ compartment buds off of a larger $Rab7^+$ vacuolar compartment. As expected, EGF is retained in the vacuolar compartment during constriction and fission (Figure 4B, 4C and Movie S5). After merging the time-lapsed images of endosome fission with the location of the tubular ER network, we could observe an ER tubule localized to nearly every fission site (96.5%: n=29 from 24 cells, Figure 4D; see also Figure S2D). In the majority of these cases (93%), the ER was positioned perpendicular to the site of fission. By line scan analysis, it becomes clear that a dynamic ER tubule moves into place to cross over and “cup” the bud just before fission occurs (compare Pre-ER to Pre-Fission scans) (Figure 4B and C). These data reveal that ER tubules are both spatially and temporally linked to the position of late endosome fission.

Next, we aimed to generate tubular late endosomes to further resolve the position of ER contact relative to the site of fission. Consistent with previous reports (Derivery et al., 2009), we could generate slightly elongated tubular Rab7-labeled late endosomes by efficiently

depleting dynamin-2 (Dnm2) by siRNA treatment (Figure 4H). Cells were also simultaneously co-transfected with mCh-Rab7 and GFP-Sec61β. Prior to imaging, these cells were pulse-labeled with EGF (conjugated to Alexa Fluor® 647) to determine whether elongated endosomes could functionally partition cargo. Live confocal fluorescence microscopy revealed that elongated endosomes in Dnm2-depleted cells were still able to uptake EGF and undergo fission while retaining EGF in the vacuolar compartment (Figure 4E and F, Movie S6). In every example recorded (100%, n=12 from 8 cells), ER tubules crossed perpendicular to the site of LE fission (Figure 4F). As before, a dynamic ER tubule slides into place just prior to the fission event (compare white and blue arrows in two left panels). We measured the mean coverage of the ER network on tubular endosomes to be 21.24% for the 12 events captured (Figure 4I and J). Thus, the average probability of ER marked fission due to chance (21.24%) is significantly lower than the measured frequency (100%) of ER marked endosome fission.

ER Tubules Contact Cargo Sorting Domains Prior to Fission

Next, we aimed to mark endosomal sorting domains prior to fission and ask if this position also coincided with the position of ER recruitment. The retromer complex sorts cargo into a domain on the late endosome that will undergo fission and traffic to the Golgi (Arighi et al., 2004; Seaman, 2004). FAM21 binds and co-localizes with these retromer-mediated sorting domains (Derivery et al., 2009; Gomez and Billadeau, 2009). We thus asked whether ER tubules co-localized with FAM21 marked sorting domains on late endosomes. Cells were transfected with markers of ER (BFP-Sec61β), late endosomes (GFP-Rab7), and the WASH complex (mCh-FAM21). FAM21 effectively partitions to both punctate and tubular structures on $Rab7^+$ late endosomes that are indicative of retromer sorting domains (Figure 5A). We tracked 165 FAM21 structures discretely localized to budding late endosome sorting domains (Figure 5B-C, Movie S7). Of these, 80% of FAM21 domains co-localize with the site of ER tubule contact over time (see example in Figure 5B). Thus, most but not all FAM21-marked retromer domains track together with ER tubules, which suggests that the ER is recruited after the sorting domain has formed.

We next observed whether the ER is present at FAM21-marked sorting domains when endosomes are undergoing fission (Figure 5D-F, Movie S8). The ER was localized to 97% of FAM21 marked fission events (n=36 from 31 cells, Figure 5G). In the example shown, it is important to note that a dynamic ER tubule becomes associated with a FAM21-marked sorting domain just prior to constriction and fission (Figure 5E, compare white and blue arrows at 15 and 20s, respectively, and see Movie S8). The temporal recruitment of ER to the position of constriction/fission is also clear by line-scan analysis (Figure 5F, see the peak in ER fluorescence at Pre-Fission). Together, these data demonstrate that ER contact is not required for retromer sorting domain formation or FAM21 recruitment, but that ER contact sites are both spatially and temporally linked to the fission events at FAM21-marked sorting domains.

We have shown that ER tubules make contact with FAM21-marked sorting domains prior to fission. We thus wondered if ER contact with endosomes requires nucleation of actin by the WASH complex. FAM21 binds to the retromer on endosomes, it is the first component of

the WASH complex to be recruited, and does so independently of other WASH complex members (Gomez and Billadeau, 2009). We could thus deplete WASH1 which will disrupt WASH complex assembly and actin nucleation (Derivery et al., 2009) and ask whether the ER is still recruited to FAM21 marked sorting domains and if so whether fission still occurs. We efficiently depleted WASH1 by siRNA and captured 25 FAM21-marked fission events where all but one localized to an ER contact site (n=25 from 21 cells, Figure S3). This demonstrates that the ER is recruited to functional endosome fission sites independent of WASH complex assembly or WASH-mediated actin nucleation.

We have shown several examples where a dynamic ER movement establishes contact with a sorting domain immediately prior to fission. ER tubule dynamics are frequent and occur on microtubules (MT) (Friedman et al., 2010; Waterman-Storer and Salmon, 1998). Thus, weprobed the effect of MT depolymerization on ER-endosome contact. Previously, we have shown that endosomes will maintain contact with the ER following MT depolymerization (Friedman et al., 2013). Here, we tested whether ER contacts would also maintain contact with endosome constrictions following microtubule depolymerization (Figure S4). We show several examples where MTs are depolymerized but ER contact still localizes to endosome constriction sites.We conclude that MT-dependent ER dynamics may be necessary to initiate contact between ER tubules and the constriction site. However, once formed, MTs do not appear necessary to maintain contact.

ER is Recruited to the Endosome Immediately Prior to Fission

We show that tubular sorting domains can be observed prior to ER contact and fission. Often ER tubules “attack” the site of the pre-formed sorting domain resulting in fission (Figure 6A and 6B). In the two complimentary examples shown, fission is observed within 10 seconds of contact formation (Figure 6A and B). Many mechanisms have been identified to form the budding domain and sort cargoes (Figure 6C). Microtubule motors have been implicated in sorting and trafficking cargoes (Hunt et al., 2013). Sorting nexins can drive the formation of budding tubules and stabilize them via curvature sensing BAR domains (Cullen, 2008). The retromer complex interacts with the sorting nexins and is involved in sorting of cargoes (Pfeffer, 2009; Seaman et al., 2013). FAM21 binds the retromer and is responsible for recruitment of remaining WASH complex components (Gomez and Billadeau, 2009). The WASH complex stimulates Arp2/3 at endosomal sorting domains thereby activating actin polymerization (Derivery et al., 2009). The presence of actin patches can also help to segregate select cargoes into the bud (Puthenveedu et al., 2010). The role of these multiple factors is to generate sorting domains to traffic cargo. Here,we show that following sorting, the ER establishes contact with the endosome at sites that are spatially and temporally linked to endosome fission.

Disruption of ER Dynamics and Shape Affects the Rate of Endosome Fission

Our data support the following order of events: the budding sorting domain forms, ER tubule contact is established at the interface between the endosome and the bud, and then ~5–10 seconds later fission occurs at this contact site (Figure 6A and B). Consistent with this model, we show several compelling examples where a dynamic ER tubule “attacks” the future fission site. Thus, our prediction was that altering the shape and dynamics of the

peripheral ER tubules would lead to a reduction in the frequency of late endosome fission. We chose to disrupt ER shape and dynamics by overexpressing human Reticulon 4a (Rtn4a), which has previously been shown to generate highly elongated and unbranched ER tubules (Shibata et al., 2008; Voeltz et al., 2006). Elongated tubules are coated with immobilized Rtn4a oligomers that can exclude other ER luminal and membrane proteins from the peripheral ER (Shibata et al., 2008; Voeltz et al., 2006; Zurek et al., 2011).

Cells were co-transfected with the general luminal ER marker BFP-KDEL, mCh-Rab7 to visualize endosome fission, and with or without high levels of Rtn4a-GFP. Compared to control, the Rtn4a-GFP cells had an altered ER morphology. As expected, the peripheral ER tubules were highly elongated, unbranched, and luminal BFP-KDEL was mostly excluded from these elongated Rtn4a-GFP tubules (Figure 7A, compare Rtn4a labelled top panels to control bottom panels). ER tubules were also significantly less dynamic with Rtn4a overexpression. This was measured quantitatively for all cells analyzed using the Pearson's correlation coefficient of overlaid 5μm square boxes from two frames taken 60 seconds apart (Figure 7B and C) (French etal., 2008).By this measurement, the time-lapse images of the ER in Rtn4a-GFP expressing cells were more co-localized over time because the peripheral ER moved less, thus resulting in a higher Pearson's correlation (control n=22, Rtn4a n=20). We tested whether the change in ER morphology caused by overexpressing Rtn4a impacted endosome fission. We recorded 2-minute movies of hundreds of individual late endosomes. For each endosome, we determined whether it formed a budding domain during the course of the movie. For each endosomal bud observed, we measured the size of the endosome, the maximum bud length, and whether it underwent fission (control n=257, Rtn4a n=257). We found that altering ER shape did not significantly affect endosome size or bud length (Figure 7D and E).However, we found that the number of buds that underwent fission was significantly reduced with Rtn4a overexpression (Figure 7F).Thus, when ER membrane composition, shape, and dynamics are altered, the process of endosome fission is defective.

Discussion

We have shown here that ER tubules form stable contact sites with sorting domains on early and late endosomes and that ER contact is a defining feature of endosome fission. These results are strikingly analogous to previous data showing that ER contact sites define the position of mitochondrial constriction and division (Friedman et al., 2011). Together, these reports demonstrate that the ER has an important and nontraditional role in the cell: to regulate the dynamics and biogenesis of at least two unique cytoplasmic organelles. How could an ER contact site regulate the constriction and/or fission of another organelle? We favor three possibilities. First, contact sites could provide a platform for the recruitment of necessary factors from each organelle that are required to drive fission. Second, since the ER is the site ofsynthesis for most phospholipids, it is possible that direct translocation of lipids from the ER into the endosomal membrane at contact sites generates a region of high lipid membrane curvature that would promote fission. The ER is also home to lipid modifying enzymes that may transform lipids on the endosomal membrane to similarly drive localized changes in membrane curvature. A third favored model is that ER stores could provide high local concentrations of Ca^{2+} required to activate a Ca^{2+}-dependent activity on the endosome

and regulate fission. Indeed, these mechanisms are not mutually exclusive and may all contribute to organelle fission at contact sites.

From an evolutionary point of view, one might think the ability of the ER to divide neighboring organelles would be advantageous for expedited ER dynamics within the cell or for whole-cell rearrangements that occur during mitosis. Both are daunting tasks considering the density of the organelles in the intracellular environment. However, the position of the ER at the site of fission appears to be purposeful for fission of endosomes as well as for mitochondria. We have observed that the ER settles to form stable contact sites with the divide between sorting compartments prior to fission. Likewise, on mitochondria, the ER is also purposefully localized to the position of nucleoid segregation prior to mitochondrial division (Murley et al., 2013).

How ER tubules bind to fission sites on endosomes (and even on mitochondria) is not known and remains an open and important question to answer. Although several partners have been identified that can bridge the apposing membranes, including PTP1B-EGFR, VAP-A-ORP1L, and STARD3-ORP1L (Alpy et al., 2013; Eden et al., 2010; Rocha et al., 2009), none have been shown to be required for maintenance of contact. Thus, these could all be independent tethers for independent functions or these complexes could function at sites that are tethered by yetunidentified factors. There are likely multiple points of contact between the ER and endosomes that could coordinate functions. For example, previous immuno-electron microscopy has also shown co-localization of EGFR and PTP1B at the ER-endosome interface (Eden et al., 2010; Haj et al., 2002). By live confocal microscopy, we also find that EGF within endosomes frequently tracks with the position of ER contact (Figure S5A). Therefore, we tested if ER-marked endosome fission occurs at the same contact sites as EGF clustering. We found that EGF puncta localized to less than half of the ER-marked fission events (Figure S5B). These data demonstrate that multiple functional and structural contact sites exist between the ER and endosomes to coordinate different functions during cargo sorting and fission. The machinery at ER-marked endosome fission sites could be especially difficult to identify because in many examples these contacts are established anew immediately prior to the fission event and thus are likely to be very transient. The identification of this transient machinery will be a next major goal.

Experimental Procedures

Plasmid Construction

GFP-Sec61β (Shibata et al., 2008), BFP-Sec61β (Zurek et al., 2010), mCh-Sec61β (Zurek et al., 2010), mCh-Rab5B (Friedman et al., 2010), BFP-Rab5B (Friedman et al., 2013), Rtn4a-GFP (Shibata et al., 2008), and mCh-aTubulin (Friedman et al., 2010) were previously described. GFP-Rab4B was a gift from A.R. English (University of Colorado-Boulder) and was generated by PCR amplifying human Rab4B (National Center for Biotechnology Information [NCBI] accession number NM_016154.4) into BglII/KpnI of pAcGFP1-C1 (Clontech, Mountain View, CA). GFP-Rab5B was a gift from J. R. Friedman (University of California-Davis) and was generated by PCR amplifying human Rab5B (NCBI accession number NM_002868.3) andcloning it into the XhoI/BamHI sites of pAcGFP1-C1 (Clontech, Mountain View, CA). To generate GFP-Rab7A, human Rab7A (NCBI accession number

NM_004637.5) was PCR amplified and cloned into XhoI/HindIII sites of the pAcGFP1-C1 vector. mCh-Rab7A was made like GFP-Rab7A but mCh was cloned into the NheI/XhoI sites of pAcGFP1-C1, replacing the GFP. mCh-FAM21and BFP-FAM21 were generated by subcloning mCh- or BFP- into the BamHI and MluI sites while removing HA-YFP from the shFAM21/HA-YFP-FAM21 rescue vector given to us by Dr. Daniel Billadeau described in Gomez and Billadeau, 2009 and Jia, et al., 2012. GFP-TfR was generated by Dr. Lois Greene.

Cell growth and plasmid DNA transfections

Cos-7 cells (ATCC, Manassas, Virginia) were grown in DMEM media (Invitrogen, Carlsbad, CA) supplemented with 10% FBS and 1% penicillin/streptomycin. Cells were seeded in a 60x15mm dish at $5.0x10^5$ cells ~16 hours prior to transfection. Cells were transfected ~24 hours prior to imaging with plasmid DNA in Opti-MEM media (Invitrogen) with 12.5 μl of Lipofectamine 2000 reagent (Invitrogen) according to the manufacturer's instructions. After ~5 hours of transfection, cells were seeded in 35mm glass-bottom microscope dishes (MatTek, Ashland, MA) at $2.0x10^5$ cells. Cells were imaged in 37°C Opti-MEM. For all experiments, the following amounts of plasmid DNA were transfected into cells for experiments: 500ng/mL BFP-Sec61β; 250ng/mL mCh-Sec61β and GFP-Sec61β; 25ng/mL GFP-Rab4; 50ng/mL BFP-Rab5 and GFP-Rab5; 125ng/mL mCh-Rab5; 20ng/mL mCh-Rab7; 250ng/mL mCh-FAM21; 500ng/mL BFP-FAM21; 165ng/mL GFP-TfR; 500ng/mL Rtn4a-GFP; 250ng/mL BFP-KDEL; 62.5ng/mL mCh-aTubulin.

RNAi transfection and Western blot

Dynamin-2 was depleted using an ON-TARGETplus Human DNM2 (1785) siRNA SMARTpool (Thermo, Waltham, MA). WASH was depleted using ON-TARGETplus Human WASH1 (100287171) siRNA SMARTpool (Thermo). Cells were seeded in a 60x15mm dish at $5.0x10^5$ cells ~16 hours prior to first transfection. Cells were first transfected ~72 hours prior to imaging with 12.5 μL Dharmafect (Thermo) in DMEM with 10% FBS and 25 nM RNAi oligonucleotides or 25 nM Silencer Negative Control #1 siRNA (Ambion AM4635). After ~6 hours of transfection, cells were washed and media was replaced with DMEM supplemented with 10% FBS and 1% penicillin/streptomycin. Cells were transfected again ~24 hours prior to imaging with plasmid DNA as described before with the addition of 25 nM RNAi oligonucleotides or 25 nM Silencer Negative Control #1 siRNA. After ~5 hours of transfection, cells were seeded in 35mm glass-bottom microscope dishes (MatTek) at $2.0x10^5$ cells. Cells were imaged in 37°C Opti-MEM.

Whole cell lysates of Cos-7 cells were resuspended in Laemmli sample buffer, boiled for 10 minutes, separated by SDS-PAGE, and transferred to a PVDF membrane. Primary antibody concentrations were used as follows: Rab7 (Cell Signaling 99367S, Danvers, MA) 1:1000; Dynamin-2 (Abcam ab3457, Cambridge, MA) 1:15,000; WASH1 (gift from D. Billadeau) 1:6000; GAPDH (Sigma-Aldrich G9545, St. Louis, MO) was used as a loading control at 1:20,000. HRP-conjugated goat anti–rabbit secondary antibody (Sigma-Aldrich) was used at 1:3000, and signal was detected with SuperSignal West Pico Chemiluminescent Substrate (Thermo). Band density was estimated using ImageJ (National Institutes of Health, Bethesda, MD) Gel Analyzer.

Confocal microscopy

Live-cell imaging was performed with an inverted fluorescence microscope (TE2000-U; Nikon, Melville, NY) equipped with an electron-multiplying charge-coupled device (CCD) camera (Cascade II; Photometrics) and a Yokogawa spinning-disk confocal system (CSU-Xm2; Nikon). Images were taken with a 100× numerical aperture 1.4 oil objective (Nikon). While imaging, live cells were kept at 37°C in a live-cell incubation chamber (Pathology Devices, Westminster, MD). Images were acquired with MetaMorph 7.0 (MDS Analytical Technologies, Sunnyvale, CA), analyzed, merged, and contrasted using ImageJ, as well as contrasted and converted to 400dpi using Photoshop (Adobe, San Jose, CA). Scale bars were generated using ImageJ. Supplemental videos were generated using ImageJ.

Endosome fission and ER coverage analysis

Cos-7 cells expressing markers for ER and endosomes were visualized live by confocal fluorescence microscopy every five seconds for two minutes in a single focal plane. Fission events were counted if they were in regions of the cell with resolvable ER tubules. Association of ER tubules was classified as adjacent, crossing, or not associated. Line-scans were performed using ImageJ by drawing a line the width of the budding compartment along the length of the entire endosome. Fission of dynasore-induced elongated endosomes (Figure 3B-D) and Dynamin-2 siRNA-induced elongated endosomes (Figure 4E-G) was analyzed if ER coverage was measured as <35% of the total endosome area.

To predict the frequency of ER at the site of fission if fission could occur at any ER crossing along the endosome, we measured the area of crossing ER tubules versus total endosome area from the image immediately preceding endosome fission for all events. The area was measured using the adaptive threshold plugin for ImageJ (created by Qingzong Tseng) which converts the 8-bit images to binary form defining the ER or endosome structure. We found the percent of endosome area covered by crossing ER tubules by comparing the number of pixels positive for ER signal to total number of pixels from the endosome area. We only selected the regions of ER that crossed the elongated endosome, omitting any ER tubules that ran parallel to the endosome.

Fluorescent cargo treatment and imaging

Prior to imaging, cells were incubated in 37°C growth media containing either 1 μg/ml EGF conjugated to Alexa Fluor® 647 (Invitrogen) or 50 μg/ml transferrin conjugated to Alexa Fluor®647 (Invitrogen) for 5–10 minutes. Then, cells were washed 2 times in 37°C Opti-MEM and imaged for less than 30 minutes to localize transferrin or EGF to early endosomes or after 30 minutes to localize EGF to late endosomes.

Dynasore treatment and imaging

Cells were passaged and transfected as described above. Cells were then washed 2 times and incubated in serum-free, antibiotic-free DMEM containing 80–160 μM dynasore (Sigma-Aldrich) for 30 minutes prior to imaging. After locating cells containing tubular endosomes by confocal microscopy, 10% FBS was added to inactivate dynasore thereby preventing adverse effects and restoring fission.

To label cargo in dynasore treated cells, cells were simultaneously incubated with either 1 μg/ml EGF conjugated to Alexa Fluor® 647 (Invitrogen) or 50 μg/ml transferrin conjugated to Alexa Fluor®647 (Invitrogen) for the duration of the dynasore incubation saturating the endosomes with cargo. Following the incubation, cells were washed 2 times with serum-free, antibiotic-free DMEM to remove excess cargo and the media was replaced with serum-free, antibiotic-free DMEM containing 80–160 μM dynasore for imaging.

Diffusion barrier identification by photobleaching

Cos-7 cells were transfected with GFP-TfR, BFP-Rab5 and mCh-Sec61β as described above. Cells were dynasore treated as described above. Once a cell containing tubular endosomes was identified, a circular region of interest 30 pixels in diameter was created using MetaMorph 7.0. Using the Mosaic Digital Diaphragm System for Nikon TE2000 Microscope (Photonic Instruments), an image was captured pre-bleach and the region of interest was photobleached for 2 seconds (Uniblitz VCM-D1 shutter, Vincent Associates) using an Argon laser with a wavelength of 450–515 nm (National Laser Company). An image was taken post-bleach followed by a 1 minute movie of all expressed channels with 5 second intervals.

To analyze the pattern of recovery and thus any barriers to diffusion, line-scans and kymographs were created using ImageJ. We identified constrictions marked by ER tubule crossings by drawing a line the width of the tubular endosome being analyzed and measuring the mean fluorescence intensity along the length of the tubular endosome.

Measuring dynamic ER movements

Live Cos-7 cells were imaged every 5 seconds for 2 minutes. Raw images taken 60 seconds apart were converted to 8-bit and overlaid using ImageJ. The average Pearson's correlation coefficient was determined for three peripheral 5μm boxes for each cell using the PSC Colocalization plugin for ImageJ (French et al., 2008). A higher degree of co-localization (Pearson's correlation coefficient closer to 1.0) between the images over time is indicative of a less dynamic ER.

Nocodazole treatment and imaging

Dynamin-2 was depleted as described above to enrich for elongated endosomes. Cells were passaged and transfected as described above. Cells were then washed and incubated in 37°C Opti-MEM prior to imaging. After locating cells containing elongated endosomes by confocal microscopy, a z-stack was acquired. Then, 5 μM nocodazole (Acros Organics) was added for at least 15 minutes or until the majority of microtubules had depolymerized. A z-stack was taken post-treatment to observe the position of the ER relative to endosome constrictions.

Supplementary Material

Refer to Web version on PubMed Central for supplementary material.

Acknowledgments

We thank J. Nunnari, J. Friedman, and L. Greene for helpful discussions. We also thank C. Merrifield, L. Greene, and G. Hajnoczky for generating plasmids used here and D. Billadeau for the FAM21 containing plasmid and the WASH1 antibody. A.A.R. is a Gordon Stone Fellow and was supported by a pre-doctoral training grant from the National Institutes of Health (GM07135). M.J.P. is supported by an NSF Graduate Research Fellowship DGE 1144083 and was supported by a pre-doctoral training grant from the NIH (T32 GM08759). This work is also supported by a Research Scholar grant from the American Cancer Society and by a grant from the National Institutes of Health (GM083977) to G.K.V.

References

Alpy F, Rousseau A, Schwab Y, Legueux F, Stoll I, Wendling C, Spiegelhalter C, Kessler P, Mathelin C, Rio MC, et al. STARD3 or STARD3NL and VAP form a novel molecular tether between late endosomes and the ER. J Cell Sci. 2013; 126:5500–5512. [PubMed: 24105263]

Arighi CN, Hartnell LM, Aguilar RC, Haft CR, Bonifacino JS. Role of the mammalian retromer in sorting of the cation-independent mannose 6-phosphate receptor. J Cell Biol. 2004; 165:123–133. [PubMed: 15078903]

Barbero P, Bittova L, Pfeffer SR. Visualization of Rab9-mediated vesicle transport from endosomes to the trans-Golgi in living cells. J Cell Biol. 2002; 156:511–518. [PubMed: 11827983]

Cullen PJ. Endosomal sorting and signalling: an emerging role for sorting nexins. Nat Rev Mol Cell Biol. 2008; 9:574–582. [PubMed: 18523436]

Derivery E, Sousa C, Gautier JJ, Lombard B, Loew D, Gautreau A. The Arp2/3 activator WASH controls the fission of endosomes through a large multiprotein complex. Dev Cell. 2009; 17:712–723. [PubMed: 19922875]

Dunn KW, McGraw TE, Maxfield FR. Iterative fractionation of recycling receptors from lysosomally destined ligands in an early sorting endosome. J Cell Biol. 1989; 109:3303–3314. [PubMed: 2600137]

Eden ER, White IJ, Tsapara A, Futter CE. Membrane contacts between endosomes and ER provide sites for PTP1B-epidermal growth factor receptor interaction. Nat Cell Biol. 2010; 12:267–272. [PubMed: 20118922]

Elbaz Y, Schuldiner M. Staying in touch: the molecular era of organelle contact sites. Trends Biochem Sci. 2011; 36:616–623. [PubMed: 21958688]

French AP, Mills S, Swarup R, Bennett MJ, Pridmore TP. Colocalization of fluorescent markers in confocal microscope images of plant cells. Nat Protoc. 2008; 3:619–628. [PubMed: 18388944]

Friedman JR, Webster BM, Mastronarde DN, Verhey KJ, Voeltz GK. ER sliding dynamics and ER-mitochondrial contacts occur on acetylated microtubules. J Cell Biol. 2010; 190:363–375. [PubMed: 20696706]

Friedman JR, Lackner LL, West M, DiBenedetto JR, Nunnari J, Voeltz GK. ER tubules mark sites of mitochondrial division. Science. 2011; 334:358–362. [PubMed: 21885730]

Friedman JR, Dibenedetto JR, West M, Rowland AA, Voeltz GK. Endoplasmic reticulum-endosome contact increases as endosomes traffic and mature. Mol Biol Cell. 2013; 24:1030–1040. [PubMed: 23389631]

Gautreau A, Oguievetskaia K, Ungermann C. Function and regulation of the endosomal fusion and fission machineries. Cold Spring Harb Perspect Biol. 2014; 6:1–16.

Gomez TS, Billadeau DD. A FAM21-containing WASH complex regulates retromer-dependent sorting. Dev Cell. 2009; 17:699–711. [PubMed: 19922874]

Haj FG, Verveer PJ, Squire A, Neel BG, Bastiaens PIH. Imaging sites of receptor dephosphorylation by PTP1B on the surface of the endoplasmic reticulum. Science. 2002; 295:1708–1711. [PubMed: 11872838]

Hanyaloglu AC, von Zastrow M. Regulation of GPCRs by endocytic membrane trafficking and its potential implications. Annu Rev Pharmacol Toxicol. 2008; 48:537–568. [PubMed: 18184106]

Harbour ME, Breusegem SY, Seaman MNJ. Recruitment of the endosomal WASH complex is mediated by the extended “tail” of Fam21 binding to the retromer protein Vps35. Biochem J. 2012; 442:209–220. [PubMed: 22070227]

Helle SCJ, Kanfer G, Kolar K, Lang A, Michel AH, Kornmann B. Organization and function of membrane contact sites. Biochim Biophys Acta. 2013; 1833:2526–2541. [PubMed: 23380708]

Hunt SD, Townley AK, Danson CM, Cullen PJ, Stephens DJ. Microtubule motors mediate endosomal sorting by maintaining functional domain organization. J Cell Sci. 2013; 126:2493–2501. [PubMed: 23549789]

Jia D, Gomez TS, Metlagel Z, Umetani J, Otwinowski Z, Rosen MK, Billadeau DD. WASH and WAVE actin regulators of the Wiskott-Aldrich syndrome protein (WASP) family are controlled by analogous structurally related complexes. Proc Natl Acad Sci U S A. 2010; 107:10442–10447. [PubMed: 20498093]

Kilpatrick BS, Eden ER, Schapira AH, Futter CE, Patel S. Direct mobilisation of lysosomal Ca2+ triggers complex Ca2+ signals. J Cell Sci. 2013; 126:60–66. [PubMed: 23108667]

Kirchhausen T, Macia E, Pelish HE. Use of dynasore, the small molecule inhibitor of dynamin, in the regulation of endocytosis. Methods Enzymol. 2008; 438:77–93. [PubMed: 18413242]

López-Sanjurjo CI, Tovey SC, Prole DL, Taylor CW. Lysosomes shape Ins(1,4,5)P3-evoked Ca2+ signals by selectively sequestering Ca2+ released from the endoplasmic reticulum. J Cell Sci. 2013; 126:289–300. [PubMed: 23097044]

Macia E, Ehrlich M, Massol R, Boucrot E, Brunner C, Kirchhausen T. Dynasore, a cell-permeable inhibitor of dynamin. Dev Cell. 2006; 10:839–850. [PubMed: 16740485]

Maxfield FR, McGraw TE. Endocytic recycling. Nat Rev Mol Cell Biol. 2004; 5:121–132. [PubMed: 15040445]

Mayor S, Presley JF, Maxfield FR. Sorting of membrane components from endosomes and subsequent recycling to the cell surface occurs by a bulk flow process. J Cell Biol. 1993; 121:1257–1269. [PubMed: 8509447]

Mesaki K, Tanabe K, Obayashi M, Oe N, Takei K. Fission of tubular endosomes triggers endosomal acidification and movement. PLoS One. 2011; 6:e19764. [PubMed: 21572956]

Morgan AJ, Davis LC, Wagner SKTY, Lewis AM, Parrington J, Churchill GC, Galione A. Bidirectional Ca^{2+} signaling occurs between the endoplasmic reticulum and acidic organelles. J Cell Biol. 2013; 200:789–805. [PubMed: 23479744]

Murley A, Lackner LL, Osman C, West M, Voeltz GK, Walter P, Nunnari J. ER-associated mitochondrial division links the distribution of mitochondria and mitochondrial DNA in yeast. Elife. 2013; 2:e00422. [PubMed: 23682313]

Park RJ, Shen H, Liu L, Liu X, Ferguson SM, De Camilli P. Dynamin triple knockout cells reveal off target effects of commonly used dynamin inhibitors. J Cell Sci. 2013; 126:5305–5312. [PubMed: 24046449]

Pfeffer SR. Multiple routes of protein transport from endosomes to the trans Golgi network. FEBS Lett. 2009; 583:3811–3816. [PubMed: 19879268]

Puthenveedu MA, Lauffer B, Temkin P, Vistein R, Carlton P, Thorn K, Taunton J, Weiner OD, Parton RG, von Zastrow M. Sequence-dependent sorting of recycling proteins by actin-stabilized endosomal microdomains. Cell. 2010; 143:761–773. [PubMed: 21111236]

Rocha N, Kuijl C, van der Kant R, Janssen L, Houben D, Janssen H, Zwart W, Neefjes J. Cholesterol sensor ORP1L contacts the ER protein VAP to control Rab7-RILP-p150 Glued and late endosome positioning. J Cell Biol. 2009; 185:1209–1225. [PubMed: 19564404]

Seaman MNJ. Cargo-selective endosomal sorting for retrieval to the Golgi requires retromer. J Cell Biol. 2004; 165:111–122. [PubMed: 15078902]

Seaman MNJ. Endosome protein sorting: motifs and machinery. Cell Mol Life Sci. 2008; 65:2842–2858. [PubMed: 18726175]

Seaman MNJ, Gautreau A, Billadeau DD. Retromer-mediated endosomal protein sorting: all WASHed up! Trends Cell Biol. 2013; 23:522–528. [PubMed: 23721880]

Shibata Y, Voss C, Rist JM, Hu J, Rapoport Ta, Prinz Wa, Voeltz GK. The reticulon and DP1/Yop1p proteins form immobile oligomers in the tubular endoplasmic reticulum. J Biol Chem. 2008; 283:18892–18904. [PubMed: 18442980]

Sönnichsen B, De Renzis S, Nielsen E, Rietdorf J, Zerial M. Distinct membrane domains on endosomes in the recycling pathway visualized by multicolor imaging of Rab4, Rab5, and Rab11. J Cell Biol. 2000; 149:901–914. [PubMed: 10811830]

Stefan CJ, Manford AG, Emr SD. ER-PM connections: sites of information transfer and inter-organelle communication. Curr Opin Cell Biol. 2013; 25:434–442. [PubMed: 23522446]

Toulmay A, Prinz WA. Lipid transfer and signaling at organelle contact sites: the tip of the iceberg. Curr Opin Cell Biol. 2011; 23:458–463. [PubMed: 21555211]

Trischler M, Stoorvogel W, Ullrich O. Biochemical analysis of distinct Rab5- and Rab11-positive endosomes along the transferrin pathway. J Cell Sci. 1999; 112(Pt 2):4773–4783. [PubMed: 10574724]

Van der Kant R, Neefjes J. Small regulators, major consequences - Ca^{2+} and cholesterol at the endosome-ER interface. J Cell Sci. 2014; 127:929–938. [PubMed: 24554437]

Voeltz GK, Prinz Wa, Shibata Y, Rist JM, Rapoport Ta. A class of membrane proteins shaping the tubular endoplasmic reticulum. Cell. 2006; 124:573–586. [PubMed: 16469703]

Waterman-Storer CM, Salmon ED. Endoplasmic reticulum membrane tubules are distributed by microtubules in living cells using three distinct mechanisms. Curr Biol. 1998; 8:798–806. [PubMed: 9663388]

Zajac AL, Goldman YE, Holzbaur ELF, Ostap EM. Local cytoskeletal and organelle interactions impact molecular-motor- driven early endosomal trafficking. Curr Biol. 2013; 23:1173–1180. [PubMed: 23770188]

Zurek N, Sparks L, Voeltz G. Reticulon short hairpin transmembrane domains are used to shape ER tubules. Traffic. 2011; 12:28–41. [PubMed: 20955502]

Article Highlights

- ER tubules are recruited to cargo sorting domains on early and late endosomes.
- Diffusion of endosomal cargo is restricted at ER marked constrictions.
- ER tubules contact early and late endosomes at the position of fission.
- Recruitment of ER tubules to sorting domains defines the timing of fission.

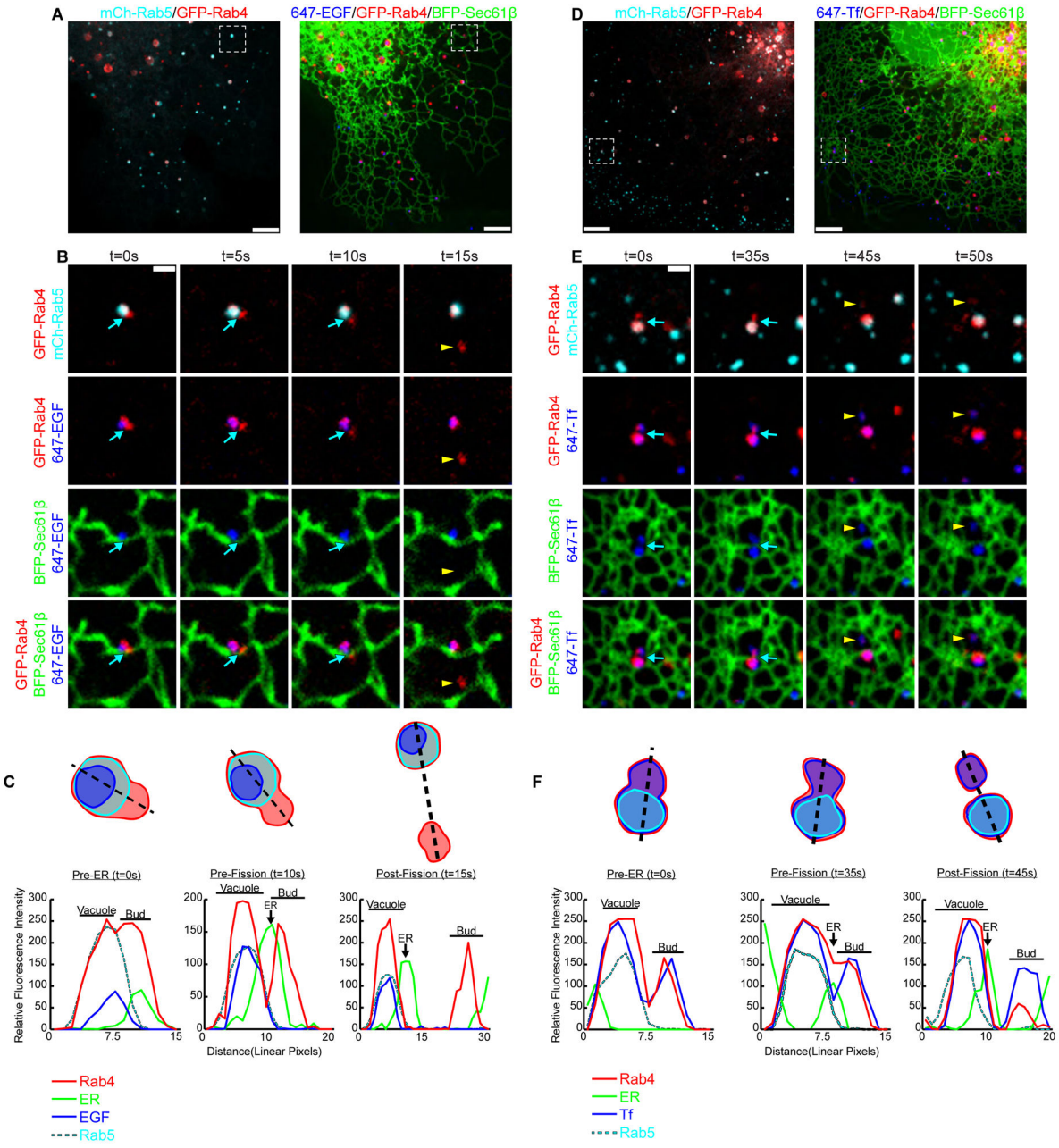

Figure 1.

Early endosome fission occurs at ER contact sites. (A) Merged images of a live Cos-7 cell expressing mCh-Rab5 (EE in cyan), GFP-Rab4 (EE in red), and BFP-Sec61β (ER in green) that is pulse-labeled with EGF conjugated to Alexa Fluor® 647 (cargo in blue). (B) Magnified time-lapse images of the region boxed in A shows an example of early endosome fission. Merged images show the relative location of Rab4, Rab5, ER and EGF, as indicated over time. The exiting $Rab4^{+}$ bud is marked by a yellow arrowhead. See also Movie S1. (C) Trace outline of the endosome shown in B and the corresponding line-scan analysis of the relative fluorescence intensity (FI) of Rab4, Rab5, ER and EGF for time points: t=0s (Pre-ER), t=10s (Pre-Fission), and t=15s (Post-fission). Images in B and line-scan in C reveal that

a dynamic ER tubule (marked by a blue arrow) is recruited to the divide between Rab4 compartments just before fission (at t=10s). (D) Merged images taken of a live Cos-7 cell transfected as in A that is instead pulse-labeled with Tf conjugated to Alexa Fluor® 647 (cargo in blue). (E) Zoom from D shows the relative localization of Rab4, Rab5, ER and Tf as indicated over time. An ER tubule (marked by blue arrow) is again recruited to the divide between Rab4 compartments just before fission (t=35s). An exiting $Rab4^{+}/Tf^{+}$ bud is marked by a yellow arrowhead. See Movie S2. (F) Line-scan analysis of relative FI depicts the position of a dynamic ER tubule to the position and timing of endosome fission for time points: t=0s (Pre-ER), t=35s (Pre-Fission), and t=45s (Post-Fission). Scale bars = 5 μm in A and D; 1 μm in B and E. s = seconds.

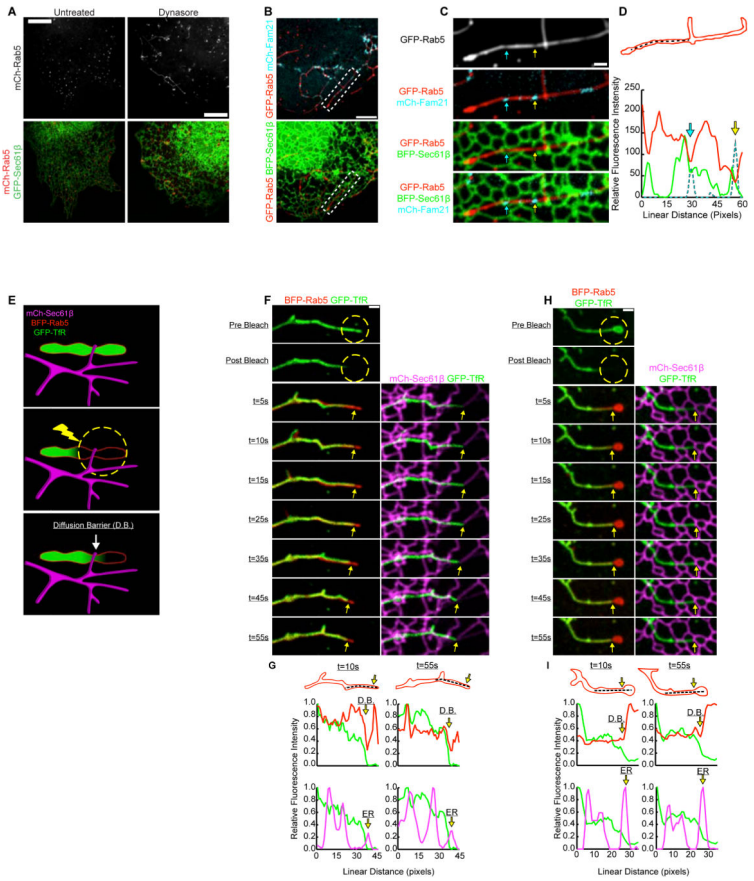

Figure 2.

ER tubules define functional constrictions along dynasore-stalled tubular endosomes. (A) Images of live Cos-7 cells expressing mCh-Rab5 and GFP-Sec61β show that dynasore treatment elongates early endosomes while ER is unaffected. (B) Merged images of live Cos-7 cells expressing GFP-Rab5, BFP-Sec61β, and mCh-FAM21 following dynasore treatment. (C) Magnified image of endosome boxed in B. Images reveal that FAM21 concentrates at positions along the tubular endosome where Rab5-labeling is reduced and ER tubules intersect these FAM21 domains. (D) Line-scan analysis of relative FI of the endosome shown in C confirms that FAM21and ER co-localize with Rab5-labeled endosome constrictions (marked by corresponding blue and yellow arrows). (E) A model outlines the FRAP technique used to test for a cargo diffusion barrier (D.B.) along tubular endosomes. (F) A live Cos-7 cell expressing BFP-Rab5, mCh-Sec61β, and GFP-TfR (membrane-bound cargo) were treated with dynasore to elongate endosomes. Endosomes were photobleached in the region indicated (dotted yellow circle). Images were taken at times indicated during the recovery (see kymograph). See also Movie S3. (G) A graph of relative FI during time points shown reveals a D.B. limits the recoveryof TfR at the position of an ER-marked constriction (at yellow arrow). The D.B./constriction maintains contact with the ER over time (marked by yellow arrows). (H-I) Another example as in F-G. Scale bars = 5 μm in A and B; 1 μm in C, F, and H.

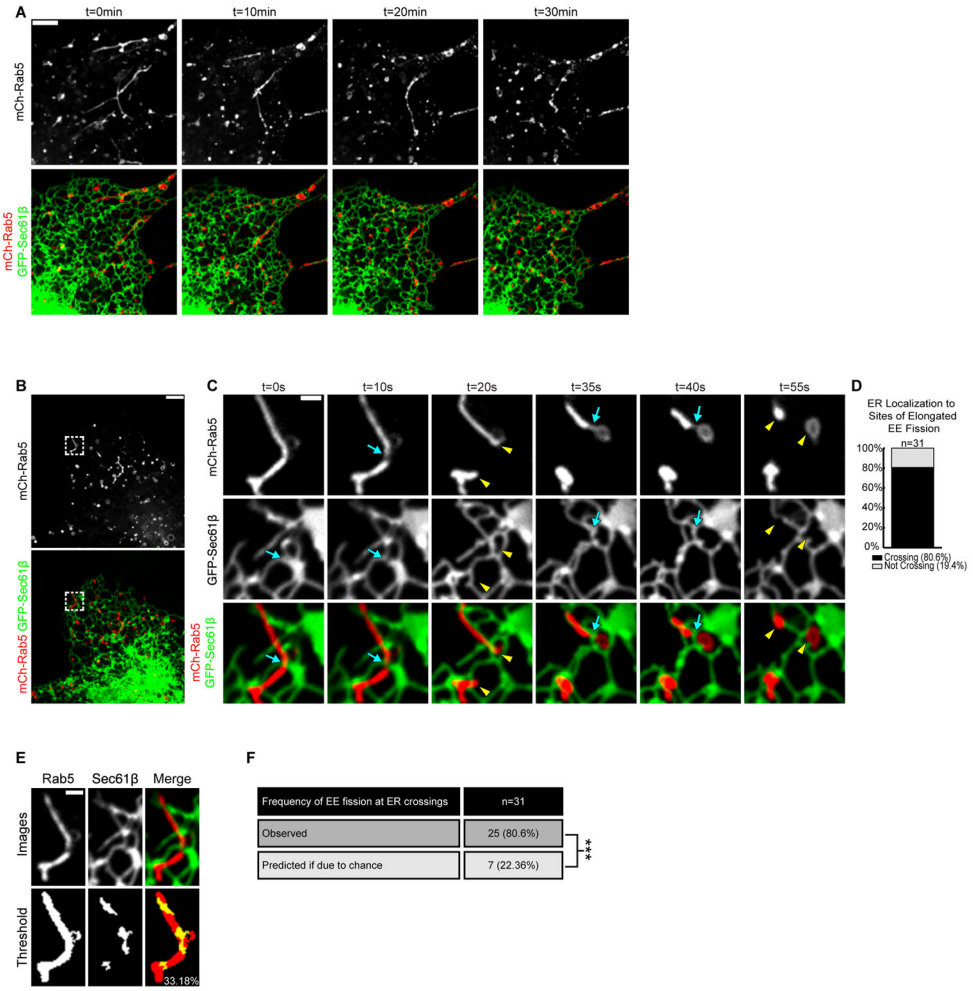

Figure 3.

Dynasore-stalled tubular early endosomes undergo fission at ER contact sites. (A) The elongated tubular endosome phenotype that results from dynasore treatment can be reversed with the addition of FBS. Time-lapsed images of live Cos-7 cells expressing mCh-Rab5 and GFP-Sec61β following dynasore treatment (t=0min) and after FBS addition at times indicated (right panels). (B)Cells treated as in A. (C) Magnified time-lapse images of region boxed in B shows two fission events that occur on a single tubular endosome with each event marked by an ER tubule crossing (blue arrows). Yellow arrowheads mark fission products after each division. See also Movie S4. (D) The percent of tubular EE fission events marked by ER tubule crossings (out of 31 events from 9 cells). (E) Method for determining the amount of endosome image surface covered by ER tubule crossing for all 31 fission events. An example is shown of endosome and ER tracing from an image immediately preceding fission. Top row shows indicated fluorescence markers and bottom row shows thresholded images. (F) Table shows the percentage (22.36%) of endosomal pixels co-localized with pixels from ER tubules crossing the endosome. The right panel shows that the measured frequency of ER-marked fission (80.6%) is significantly higher than that due to chance (22.36%). ***, P<0.001, Fisher's exact test. Scale bars = 5 μm in A and B; 1 μm in C and E. min = minutes.

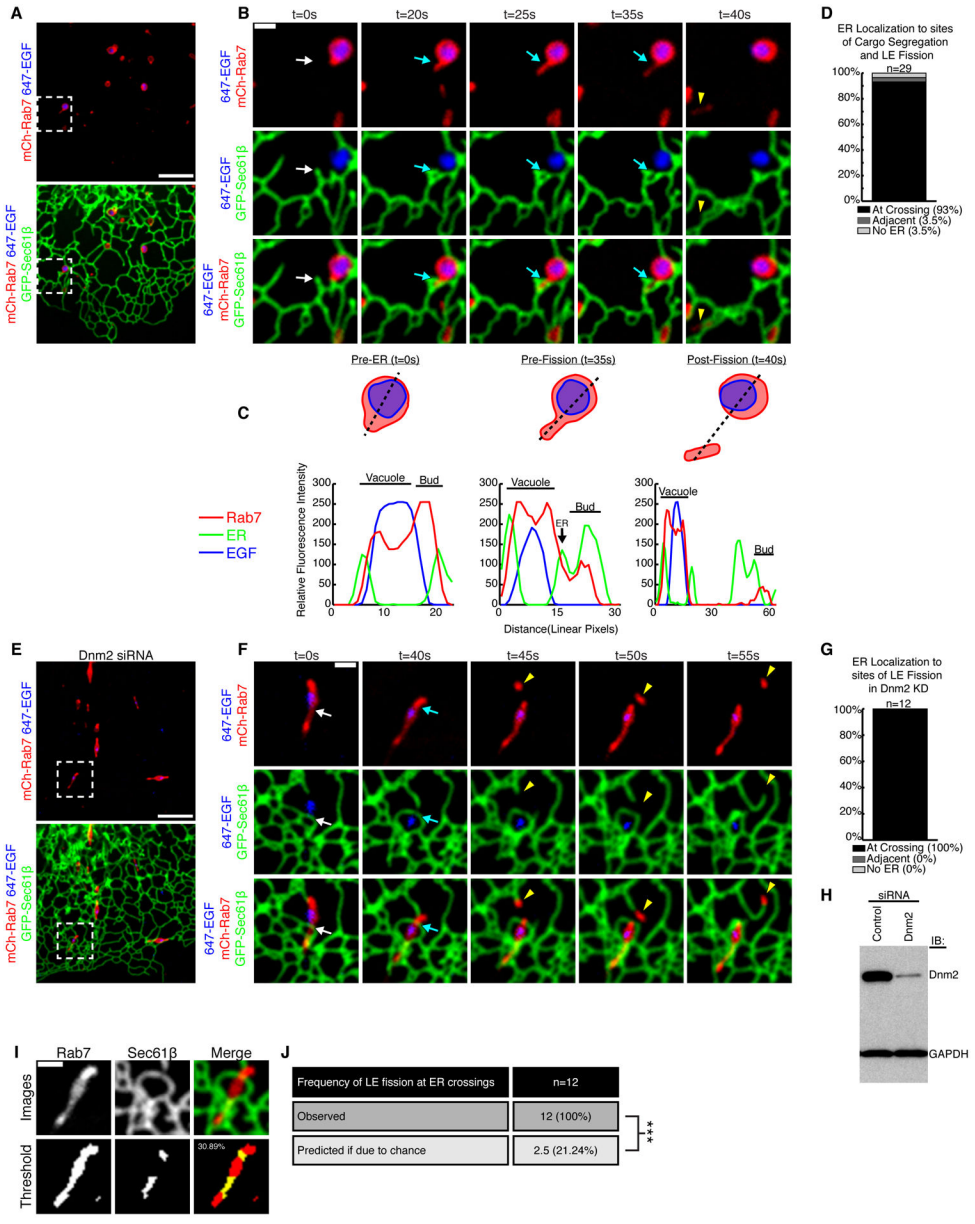

Figure 4.

Late endosome division occurs at ER contact sites. (A) A Cos-7 cell expressing mCh-Rab7 (late endosome) and GFP-Sec61β was pulse-labeled with EGF conjugated to Alexa Fluor® 647 (cargo in blue). (B) Magnified image of the region boxed in A shows an example of lateendosome fission. Merged images show the relative location of Rab7, EGF and the ER, as indicated over time. See also Movie S5. (C) Traced outline and the corresponding line-scan analysis of relative FI through the equator of the dividing endosome shown in B. Relative FI of Rab7, ER, and EGF were performed for time points: t=0s (Pre-ER), t=35s (Pre-fission), and t=40s (Post-fission). Note that a dynamic ER tubule is recruited to the position and timing of endosome constriction and fission (compare position of the ER tubule marked by an arrow at t=0s to t=20s in B and C). (D) Percent of late endosome division

events that co-localize with ER tubules (n=29 from 24 cells). (E) Image of a Dnm2-depleted cell expressing mCh-Rab7 (red) and GFP-Sec61β (green) and pulse-labeled with EGF conjugated to Alexa Fluor® 647 (blue). (F) Magnified image of box in E shows an elongated endosome that moves until it becomes associated with an ER tubule (white arrow) at the site of endosome division (blue arrow). The location of the Rab7 endosome bud (yellow arrowhead) is shown. See also Movie S6. (G) The percent of late endosome fission events that co-localize with ER tubules in the absence of dynamin-2 (out of 12 events from 8 cells). (H) Immunoblot analysis shows efficient depletion of Dnm2 in cells transfected with Dnm2 siRNA (right lane) relative to control (left lane). (I) The endosome image surface covered by ER tubule crossing was measured for all 12 fission events. In example shown, the top row shows indicated fluorescence markers and bottom row shows thresholded images. (J) Table summarizes predicted frequency of ER-marked LE fission (21.24% based on coverage) versus the actual frequency of ER-marked fission (100%). ***, $P<0.001$, Fisher's exact test. Scale bars = 5 μm in A and E; 1 μm in B and F.

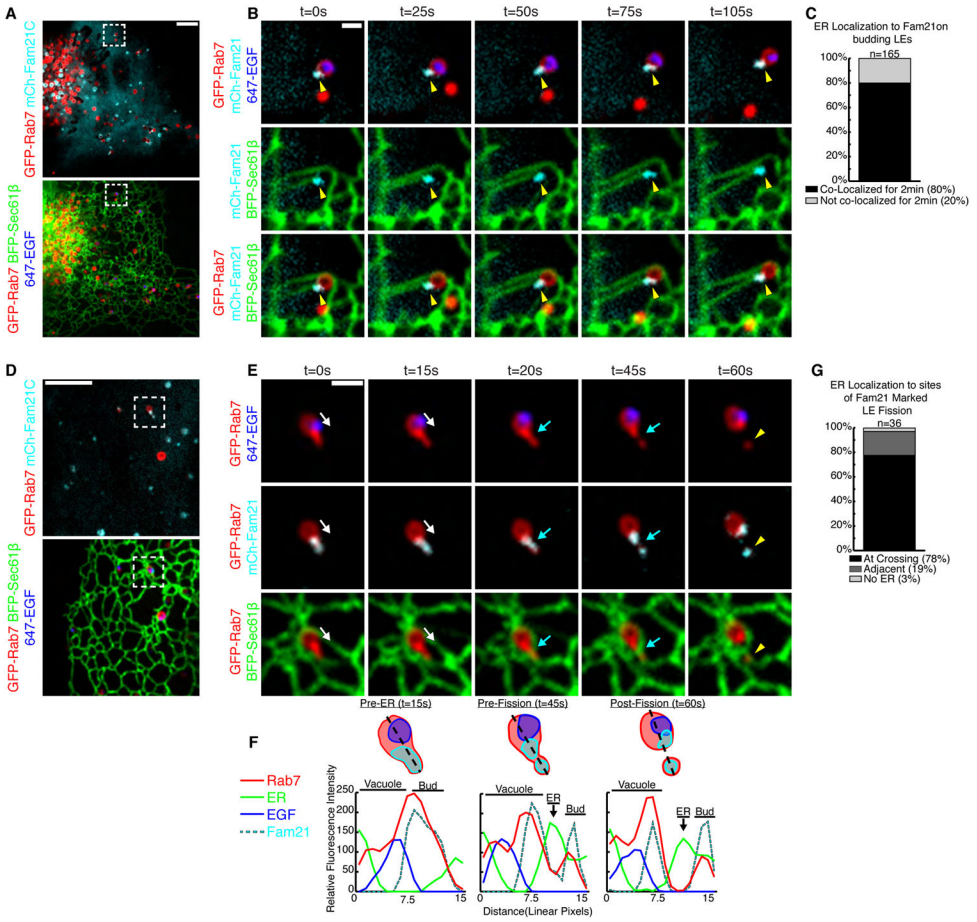

Figure 5.

The ER is recruited to FAM21-marked sorting domains prior to fission. (A) Merged image of a live Cos-7 cell expressing GFP-Rab7, BFP-Sec61β, and mCh-FAM21 that was also pulse-labeled with EGF conjugated to Alexa Fluor® 647 (cargo in blue). (B) Magnified time-lapse images of an endosome in A shows the tip of an ER tubule tracking with a FAM21 punctum at the bud of a late endosome (yellow arrowhead). See also Movie S7. (C) The number of FAM21 puncta on late endosome buds that maintain contact with ER over a 2 min time course (165 puncta from 31 cells). (D) Merged image of a live Cos-7 treated as in A. (E) Magnified images of boxed region in D shows a late endosome undergoing fission. A bud labeled by FAM21 extends from the late endosome and undergoes constriction and division. An ER tubule (follow white arrow) is recruited to the FAM21 bud just before fission (at the blue arrow). The location of the exiting Rab7 endosome bud is marked by a yellow arrowhead. See also Movie S8. (F) Line-scan analysis of endosome shown in E relates the timing and position of ER tubule recruitment relative to Rab7, FAM21, and EGF. (G) The percent of FAM21-marked late endosome division events that co-localize with ER tubules during cargo segregation, (n=36 from 31 cells). Scale bars = 5 μm in A and D; 1 μm in B and E.

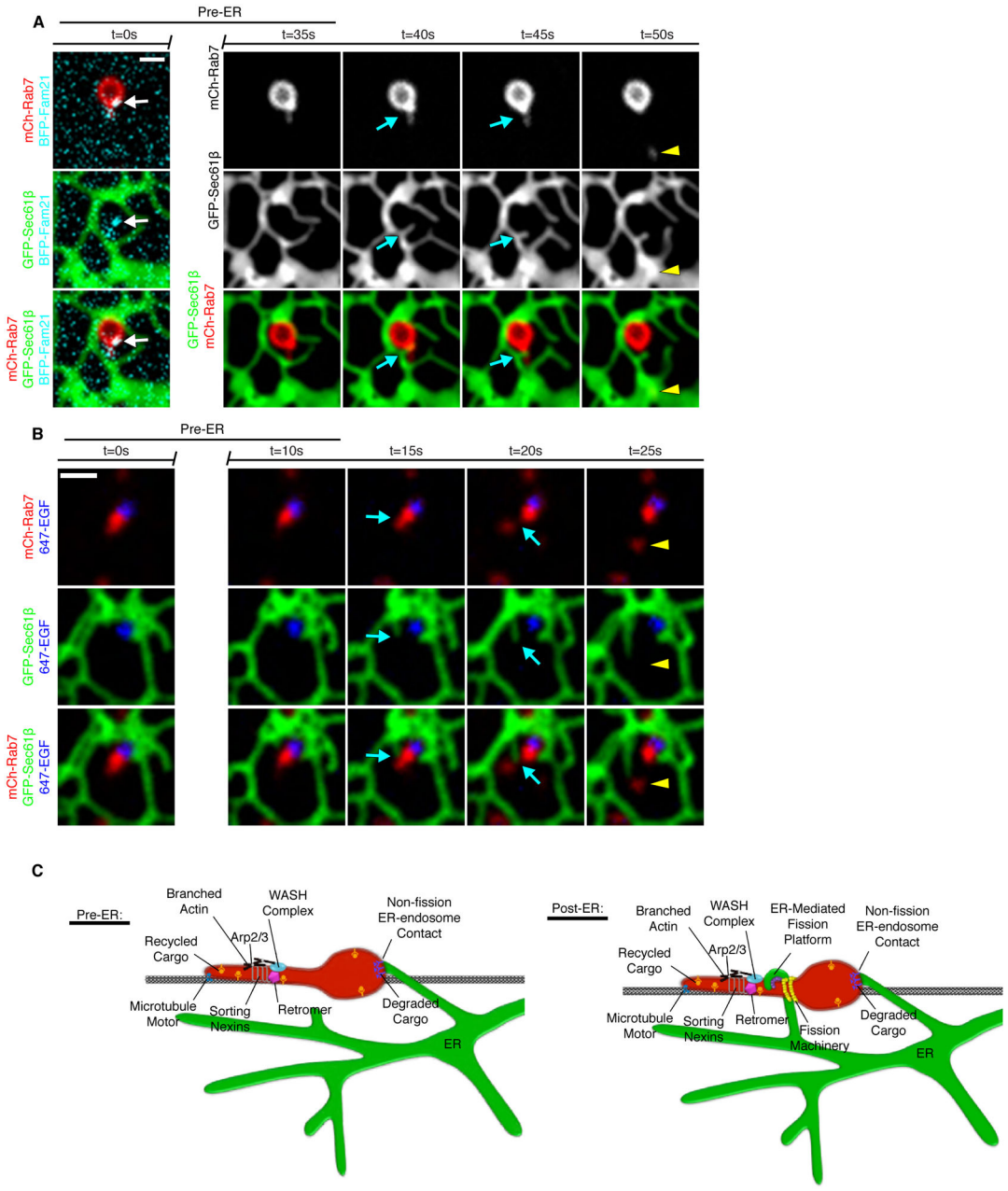

Figure 6.

Model of endosome sorting and fission factors. (A) A live Cos-7 cell expressing GFP-Rab7, mCh-Sec61β, and BFP-FAM21.Endosome fission occurs after a dynamic ER tubule contacts the endosome at a constricted sorting domain. (B) A Cos-7 cell expressing mCh-Rab7 and GFP-Sec61β was pulse-labeled with EGF conjugated to Alexa Fluor® 647.The ER tubule contacts the endosome, fission occurs at the point of contact, the budding domain leaves, maintaining ER contact. (C) The many factors implicated in endosome sorting and fission are indicated in the model pre- and post-ER recruitment. Following sorting, the ER establishes contact with the endosome at sites that are spatially and temporally linked to endosome fission.

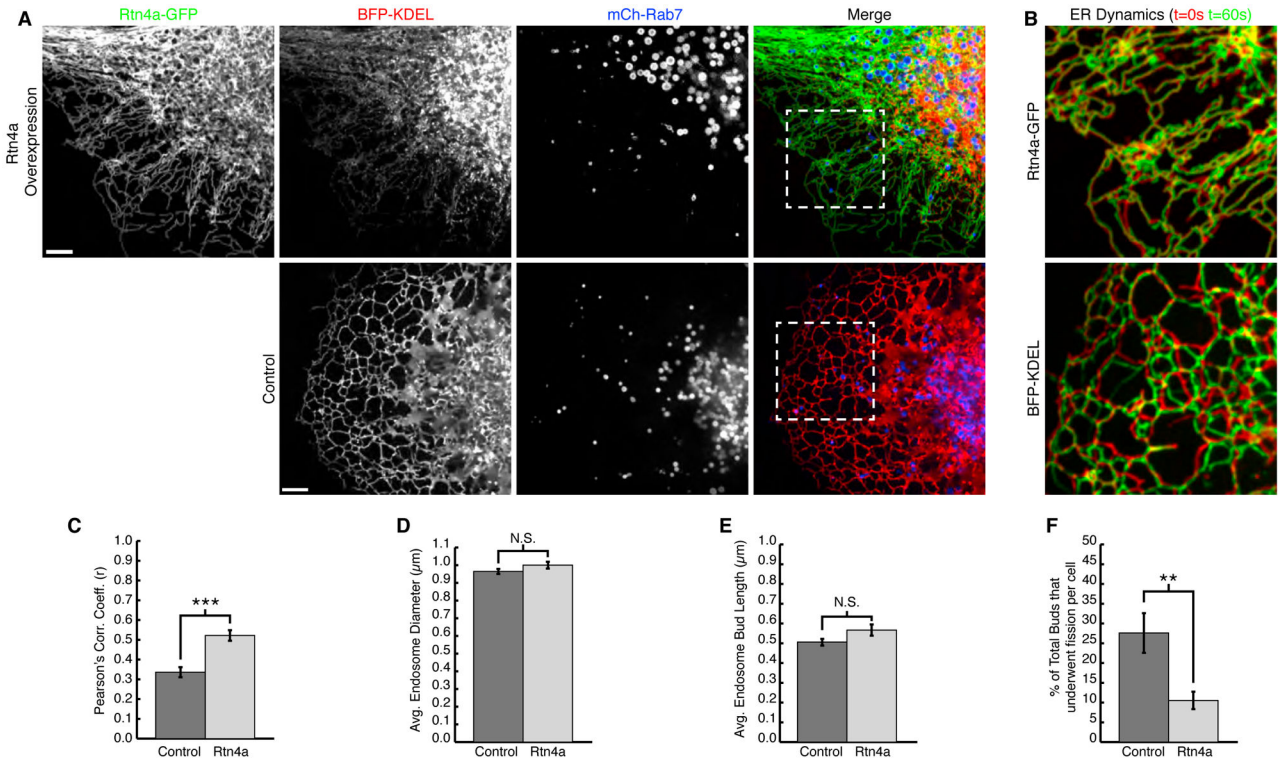

Figure 7.

ER structure and dynamics affect endosome fission. (A) Live Cos-7cells expressing BFP-KDEL and mCh-Rab7 with (top panel) or without (bottom panel) Rtn4a-GFP. Note that Rtn4a-GFP tubules are less branched (top first panel) and exclude KDEL from the periphery (top second panel). (B) Zoom from A shows overlay of t=0sec (red) with t=60sec (green) to show ER movement over time “dynamics”. (C) Graph of average Pearson’s correlation coefficient shows greater co-localization and therefore fewer dynamic ER movements for Rtn4a expressing cells (control n=22 cells, Rtn4a n=20 cells, ***, $p<0.001$, two-tailed test). (D) Graph showing no significant difference in endosome diameter between control and Rtn4a expressing cells (control n=216 endosomes, Rtn4a n=215 endosomes). (E) Graph showing no significant difference in endosome bud length between control and Rtn4a expressing cells (control n=257 buds in 22 cells, Rtn4a n=257 buds in 20 cells). (F) Graph showing a significant (**, $p<0.01$, two-tailed test) decrease in the percent of endosome buds from E that undergo productive fission in Rtn4a expressing cells. Scale bars = 5μm in A, and 1μm B and G. Error bars represent SEM.